Experimentální Analýza Napětí 2007

NEUTRON DIFFRACTION STUDIES OF INTERNAL STRESSES IN POLYCRYSTALLINE MATERIALS

Petr Lukáš, [1] Miroslav Vrána, [1] Pavol Mikula, [1] Jozef Vleugels, [2] Guy Anné, [2] Omer Van der Biest, [2] Anna Hojná[3] and Luboš Mráz[4]

Abstract: *In last two decades, the high-resolution neutron diffraction method has become well established experimental tool in non-destructive studies of internal stresses in various polycrystalline materials. Due to high penetration ability of thermal neutrons into most materials, the detailed maps of residual stresses can be measured even in relatively massive engineering components. Principles of this experimental method as well as application examples are given in this paper.*

Keywords: *neutron diffraction, nondestructive method, residual stress*

1. Introduction

X-ray diffraction method of measurement of residual stresses has been widely used in materials science and engineering for many decades, however, the practical application of this technique has been always connected with many difficulties. Because X-rays penetration depth is of about 5-10 μm, only limited surface stress information is available. It is very well known that surface stress state can be easily influenced by many external conditions, such as a surface treatment, corrosion, etc. Obtaining relevant information on surface stress state corresponding to near surface layer or bulk could be a rather difficult task in many cases.

Neutron diffraction method for determination of residual stresses has been developed at the beginning of nineties and since that time it has become very well established experimental technique in neutron research laboratories [1,2]. Due to a high penetration ability of thermal neutrons into the most of materials, this method can be used for nondestructive 3D mapping of residual stresses in bulky materials, even in large engineering components after different technological treatment. Recently, this method has been modified also for *in situ* mechanical and combined thermomechanical testing of materials.

---

[1] RNDr. Petr Lukáš, CSc., RNDr. Miroslav Vrána, CSc., RNDr. Pavol Mikula, DrSc. Nuclear Physics Institute CAS and Research Centre Řež Ltd, 250 68 Řež, Czech Republic, tel.: +420 220941147, e-mail: lukas@ujf.cas.cz

[2] Prof. Dr. ir. Jozef Vleugels, Dr. Guy Anné, Prof. Dr. ir. Omer Van der Biest, Katholieke Universiteit Leuven, Department of Metallurgy and Materials Engineering, Kasteelpark Arenberg 44, B-3001 Leuven, Belgium , tel.: +32 16321244, e-mail: jozef.vleugels@mtm.kuleuven.ac.be

[3] Dr. Anna Hojná, Nuclear Research Institute Řež p.l.c., 250 68 Řež, Czech Republic, tel.: +420 266173549, e-mail: bro@ujv.cz

[4] Ing. Luboš Mráz, PhD., Welding Research Institute - Industrial institute of Slovak Republic, Račianska 71, 832 59 Bratislava 3, Slovak Republic, tel.: +421 249246560, e-mail: mrazl@vuz.sk

2. Principles

This experimental technique employs the crystal lattice plane as a built-in microscopic strain gauge. The diffraction stress/strain measurement consists thus in the precise determination of the d_{hkl}-spacing of particularly oriented crystal planes (see Fig.1). The neutrons from this gauge volume are diffracted by a family of lattice planes (*hkl*) under the scattering angle of $2\theta_{hkl}$ according the Bragg law

$$2d_{hkl} \sin \theta_{hkl} = \lambda \tag{1}$$

where λ is the neutron wavelength. Then, the differentiated Bragg equation gives a relative lattice strain ε_{hkl} in the form

$$\varepsilon_{hkl} = \frac{d_{hkl} - d_{0,hkl}}{d_{0,hkl}} = \frac{\Delta d_{hkl}}{d_{0,hkl}} = -\cot \theta_{hkl} \Delta\theta_{hkl} \ , \tag{2}$$

where θ_{hkl} is the Bragg angle, d_{hkl} is the measured interplanar spacing and $d_{0,hkl}$ is the stress-free interplanar spacing. The strain determination is then based on measurements of angular deviation of the profile position $\Delta\theta_{hkl}$ from this value related to the stress-free state. A correct determination of $d_{0,hkl}$ is a principal problem of neutron diffraction techniques dedicated to strain measurements. As can be seen from schematic sketch in Fig.1, the diffraction evaluated strains are: i) elastic strains only, ii) determined selectively only from those grains of the specimen which are suitably oriented, iii) averaged strain values over those grains, and iv) generally only one component of the elastic strain tensor can be evaluated from a diffraction experiment with a single specimen orientation with respect to the scattering vector.

In general, the measured quantity in the diffraction experiment is the lattice strain component. For determination of the stress tensor components, Hooke's law can be used. For diffraction experiments, the expression for σ_x stress component can be written in the form

$$\sigma_x = \frac{E_{hkl}}{(1-2\nu_{hkl})(1+\nu_{hkl})}\left[(1-\nu_{hkl})\varepsilon_x^{hkl} + \nu_{hkl}(\varepsilon_y^{hkl} + \varepsilon_z^{hkl})\right] \ , \tag{3}$$

where $\varepsilon_{x,y,z}^{hkl}$ is the *x,y,z*-component of the lattice strain measured on the crystal lattice planes *(hkl)*, E_{hkl} and ν_{hkl} are the diffraction elastic Young modulus and diffraction Poisson ratio, respectively. The $\varepsilon_{x,y,z}^{hkl}$ lattice strain components are determined in the neutron diffraction experiment. Corresponding relations for other *y* and *z* stress components are obtained by simple permutations of *x,z* and *y* indexes.

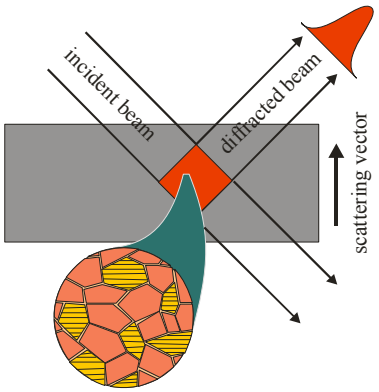

Fig. 1. Schematic sketch of the measurement of the lattice spacing parameter.

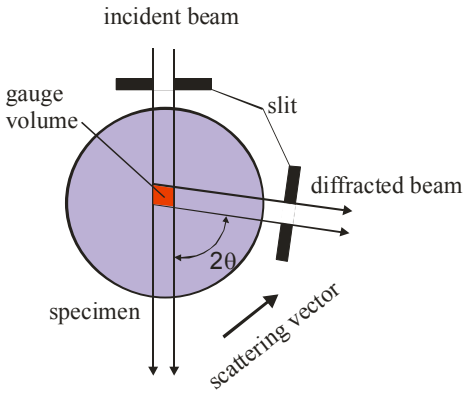

Fig. 2. The arrangement used for scanning of internal strains within the specimen bulk.

Mapping of the internal stresses in the whole volume of the specimen is performed in the experimental arrangement shown in Fig. 2. Two fixed slits in the incident and diffracted beam, respectively, are used for defining the gauge volume. The specimen is then moved step by step in the *x,y,z* directions and the corresponding diffraction spectra are collected in each position. The corresponding component of the strain tensor is adjusted by a proper rotation of the specimen with respect to the scattering vector. In such a way, the whole map of the stress/strain tensor can be received.

3. Instrumentation

In principle, any current neutron powder diffractometer can be modified for the purpose of determination of internal stresses, however, a higher instrumental resolution is required to be able to distinguish relative deformations in the range of about 10^{-5}-10^{-4}. For example, two high-resolution neutron diffractometers [3,4] dedicated to strain measurements (TKSN 400 and SPN100, see Fig. 3) are available at the medium-power reactor LVR-15 in NPI Řež. The instruments are equipped with curved Si and Ge monochromators and with linear high-resolution position-sensitive detectors for fast recording of diffraction profiles. The elastically bent perfect crystal monochromators work as a focusing element enabling to adjust an optimum high $\Delta d/d$-resolution (~2×10^{-3}). Both stress scanners can be equipped with a special dedicated shielding box enabling safe manipulation with highly radioactive specimens [5]. Moreover, the strain scanners can be optionally equipped with a deformation rig enabling both tensile and compressive tests up to maximum loading of ±20 kN. The setup can be also equipped with the hot air heating system (up to 250°C) and electric resistive heating

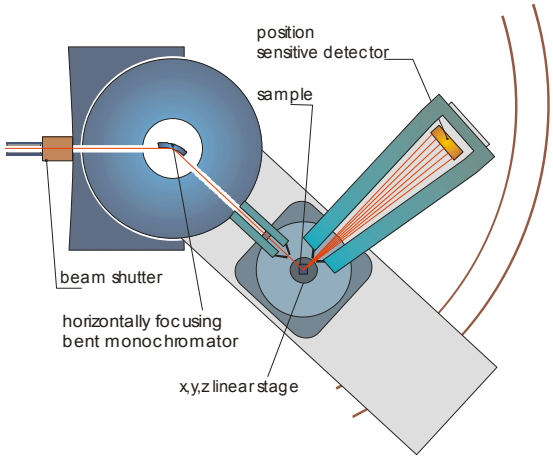

Fig. 3. An example of the neutron stress scanner – the schematic sketch of the diffractometer SPN-100 in NPI Řež.

(up to 1000°C). This auxiliary equipment makes possible *in situ* thermomechanical tests of different kind of materials [6,7].

4. Application examples

4.1 Investigation of stress fields around weld joints

Welding process introduce a relatively very strong stresses into metallic materials which could influence significantly a functional life of welded components. These stress fields can play a significant negative role in initiation and propagation of cracks appearing e.g. as a result of the operational fatigue. Minimization of stresses produced by welding is thus of a great importance. This task can be solved by an optimization of the welding technologies and/or post welding treatment of the material. Of course, a reliable experimental method for characterization of residual stresses in the vicinity of weld joints is necessary when solving this task.
As a demonstration of application possibilities of the neutron diffraction technique, we are reporting the study of residual stresses around the weld joint of the construction high-strength ferritic steel WELDOX700. The chemical composition of the base and weld material is given in Tab. 1, 2.

Table 1. Chemical composition of the WELDOX700 steel (weight %).

C	Si	Mn	P	S	Cr	Ni	Mo
0.144	0.314	1.004	0.006	0.0013	0.372	0.057	0.019

V	Ti	Cu	Al	Nb	B	N	Ca
0.047	0.015	0.016	0.043	0.020	0.0015	0.005	0.0024

Table 2. Chemical composition of the weld metal (weight %).

C	Si	Mn	P	S	Cr	Ni	Mo
0.102	-	0.76	-	-	0.27	3.94	0.24

The residual stresses produced by manual metal arc welding using cover electrodes were examined in the model specimen of the welded plate. The schematic sketch of this specimen including dimensions, definition of the used coordinate system and localization of the measuring points is given in Fig. 4. The result of the neutron diffraction experiment is summarized in Fig. 5. Three components of the residual strain were measured along the line perpendicular to the weld joint in the model sample of the welded plate. The corresponding stresses are calculated according to the Eq. 3. The diffraction elastic constants E_{hkl} and ν_{hkl} used in the formula (3) were determined in the independent experiment. Because the diffraction measurement of residual strains is based on the precise determination of the lattice parameter, the correction for stress- free lattice parameter of the used weld metal had to be performed. Otherwise the small variation in lattice parameter due to chemical composition

would be misinterpreted as a residual strain. For this purpose, a thin slice of the plate was cut perpendicularly to the weld line. This slice was further cut into small cubes of the edge size of ~4 mm. The macroscopic residual stresses are supposed to be fully relaxed in these cubes. This assumption is supported both by the FEM model and experimental diffraction verification - no variation in measured *d*-spacing values is observed in arbitrary different orientation of the cube with respect to the scattering vector.

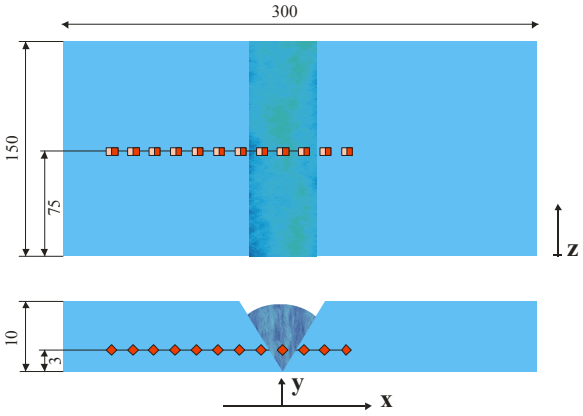

Fig. 4. Schematic sketch of the welded plate specimen, used system of coordinates and localization of the measuring points.

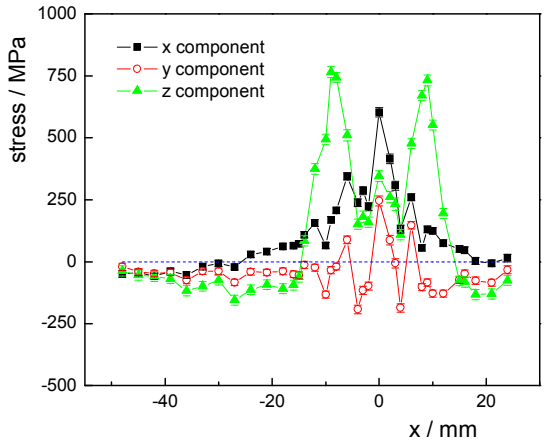

Fig. 5. Three components of the residual stress scanned along the line perpendicular to the weld point.

The significant level of residual tensile stresses of 800 MPa is detected in the vicinity of the weld joint in the stress component parallel to the weld line. The reported result is only a fragment of systematic studies of weld joints of WELDOX steels and more detailed discussion of this result exceeds the scope of this paper.

4.2 Internal stresses in functionally graded alumina/zirconia ceramics

The graded Al_2O_3/Y-ZrO_2 ceramics [8] combining excellent properties of alumina (low wear rate, high hardness) and zirconia (high strength and toughness) are developed as a prospective material for medical applications like hip and/or knee prosthesis. It is expected that an optimization of the residual stress distribution in the final products can significantly increase their performance. The challenging task for material designer is to achieve favorable compressive stresses at the working surfaces of such a component. The main source of residual stresses in Al_2O_3/Y-ZrO_2 ceramics is the thermal stress due to different thermal expansion coefficients of both phases which is induced by cooling from sintering temperature. The stress distribution can be then tailored by an appropriate variation of the phase composition [9].

The studied graded ceramics were prepared by electrophoretic deposition /EPD/ [10] followed by sintering in air for 1 hour at 1550^{o}C and hot isostatic pressing /HIP/ for 20 minutes at 1390^{o}C and 140 MPa. Parameters of the production process were optimized on testing specimens of a disc form of 35 mm in diameter and 5 mm thick (see Fig. 6). The EPD process was used to reach precise phase concentration profile. The depth profile of the alumina volume fraction shown in Fig. 8, was designed theoretically to generate compressive surface

stress of 100 MPa. To verify this prediction experimentally, the non-destructive neutron diffraction mapping of residual strains has been applied, however, because of two-phase composition of the material, a special concept had to be adopted. In the studied ceramics, the lattice strains are detected in each constituent phase individually and experimentally observed values of lattice strains reflect a superposition of both phase specific strains and macroscopic residual strains. The theoretical and experimental procedure for separation of the phase specific strains and macroscopic residual strains is described in Ref [11] in detail. The procedure was tested on the model case of flat FGM disc and, consequently, this method was applied on the final product, all-ceramic bearing of the hip prosthesis (see Fig. 7.).

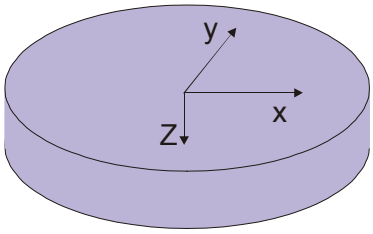

Fig. 6. Flat FGM disc and introduction of the system of coordinates in the disc.

Fig. 7. Photograph of the all-ceramic bearings of the hip prosthesis.

The result of scanning macroscopic residual stresses through the flat FGM disc is displayed in Fig. 8. Note that the compressive residual stresses of about 100 MPa were detected at the working surface. This is in excellent agreement with the theoretical prediction and FEM simulations. The profile of the residual macroscopic stresses scanned through the ball-head of the FGM ceramic hip prosthesis is presented in Fig. 9. Also in this case, the favorable compressive residual stresses of about 100 MPa were confirmed at the working surface of the ball head. The presented results demonstrate that neutron technique is able to provide very complex information on stress state of such a relatively complicated system of composite ceramics.

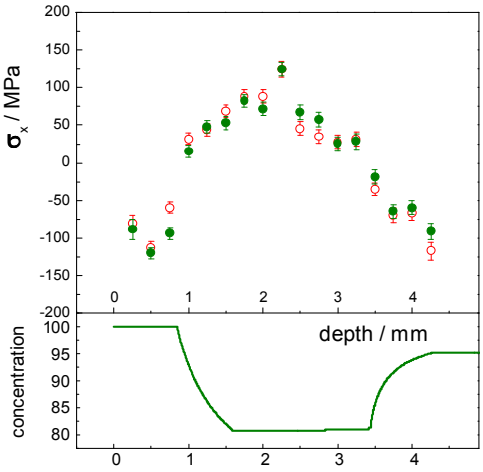

Fig. 8. Scanned residual stresses through the FGM disc. Full and empty symbols denote the independent measurements. The phase composition profile is plotted in bottom part of graph.

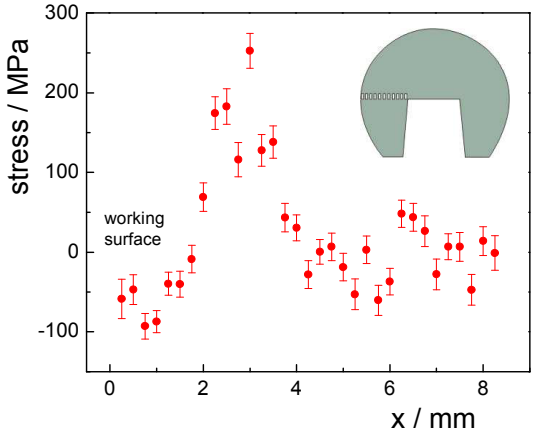

Fig. 9. The residual stresses scanned through the ball-head of the hip prosthesis. The localization of measuring points is shown in the inserted scheme.

4.3 Internal residual stresses in highly radioactive materials

Mechanical properties of construction materials used in nuclear engineering can be strongly influenced by radiation damage causing their degradation during service. From the safety point of view, the most critical items are reactor construction steels, especially the weld joints of reactor internal technological components. Knowledge of evolution of residual stress level in the dependence on time and neutron fluence is very important for assessment of the component integrity and for a support of the operation prolongation. Non-destructive scanning of residual stresses around weld joints, both in as produced and used components, is thus of a great importance because the level of the residual stresses is a limiting factor for the internal safety operation. Employing of the neutron diffraction method is then very attractive, however, the standard experimental equipment should be modified with respect to the high radioactivity of the irradiated specimens. For this purpose, a special shielding box was developed in NPI to extend the experimental resources of existing stress/strain neutron diffractometers TKSN400 and SPN100. This dedicated facility enables us an easy specimen installation in the hot cells and a remote control of specimen positioning and beam shutters and collimators. Employing this shielding box, the stress mapping experiments on radioactive

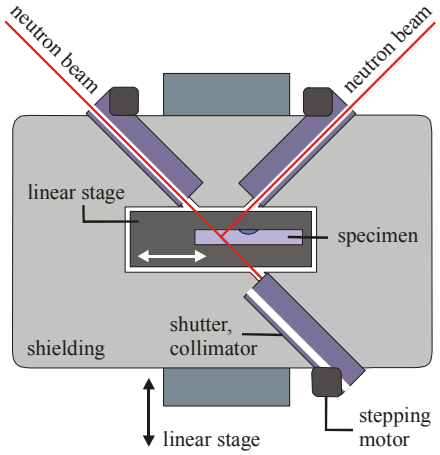

Fig.10. Schematic sketch of the experimental shielding container for strain/stress scanning of the irradiated specimens.

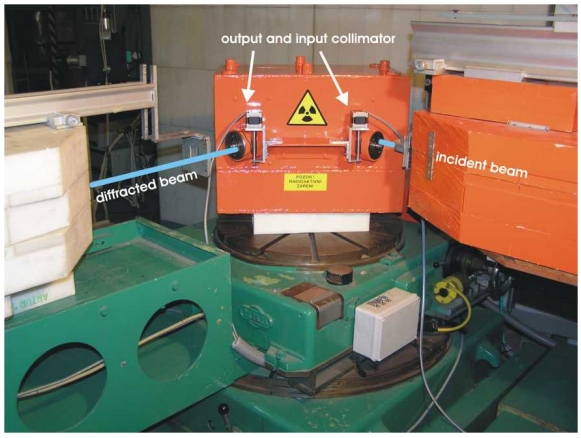

Fig. 11. Photograph of the container at the SPN100 diffractometer in the reactor hall of the reactor LVR-15.

components can be then realized by means of the current stress/strain scanners.
The schematic sketch and photograph of the dedicated shielding box is shown in Figs.10, 11. The lead container body is designed with the effective shielding layer of 16 cm. This shielding capacity would be sufficient to work with irradiated austenitic specimens up to maximum activity of 4 10^{12} Bq. The internal space of the container is equipped with a linear stage and a specimen holder. Three independent beam shutters and collimators controlled by stepping motors are used for the incident and diffracted neutron beams in transmission and reflection geometry, respectively. The rotating steel collimators provide a circular channel of the diameter of 1cm. The input and output beam were formed by Cd-masks of a size of 3x3 mm^2. The strain determined in such a diffraction experiment is then averaged over the gauge volume of 3x3x3 mm^3.
For the compliance test of the new facility we used an irradiated specimen of ongoing project of the VGB group, aimed on investigation of irradiation assisted cracking (IASCC) of

austenite steel in NRI LWR-15 reactor water loop. The tested CT specimens were manufactured from the steel A347 weld joint sample. The material sample had been cut from the circumferential weld joint of the BWR core shroud. The CT specimens of notch length of 20 mm were machined to have the fracture plane in heat-affected zone of the weld joint (Fig.12).

Table. 3. Chemical composition of used steel (wt.%)

C	Si	Mn	P	S	Cr	Ni	Nb	Co
0.031	0.57	1.27	0.016	0.012	17.10	9.30	0.52	0.040

At first, the CT specimen was irradiated in experimental reactor LWR-15 to 6.2 10^{20} n/cm^{-2}, then tested inside the in-pile reactor water-loop BWR-2. At the same time the specimen was loaded, first using cyclic and then constant load regime. After the tests the specimen was final fractured by fatigue at room temperature in air. The half of the CT specimen containing the base metal was further used for the neutron diffraction experiment. The dose rate of 2 Svh^{-1} was measured at the distance of 5 cm from the specimen surface, the total specimen activity was determined as 11 GBq.

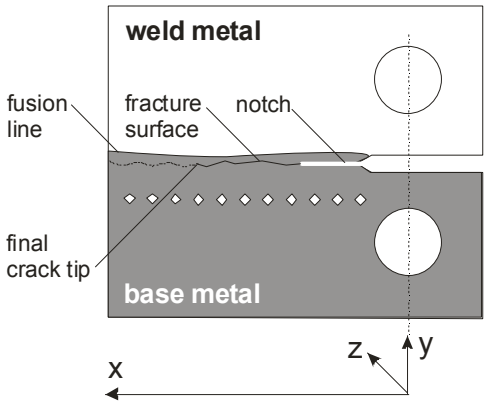

Fig. 12. Schematic drawings of the CT specimen, white squares near fracture surface indicate a location of the measuring points.

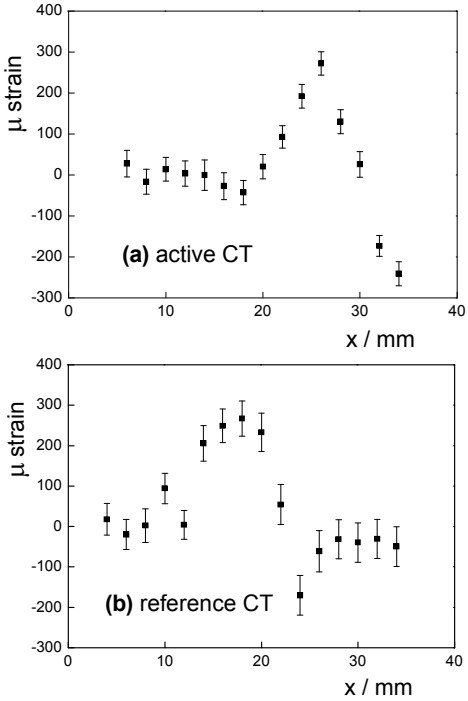

Fig.13a, b. Scan of the residual strain component perpendicular to the fracture surface in the active specimen (a) and the reference specimen (b).

The irradiated specimen in a transport container was delivered into the hot cell of the LVR-15 reactor. Here, the specimen was installed into the experimental container which was afterwards transported directly to the reactor hall and installed at the corresponding spot of the neutron diffraction facility. The first results of testing experiments at irradiated CT specimen of austenitic stainless steel are presented. In the case of diffraction measurements of residual strains in austenitic stainless steels, the most convenient reflection seems to be 311 reflection

due to the linear response of the dependence (σ, ε_{311}) even beyond the yield point [12]. To employ the austenite 311 reflection for this kind of the experiment, we used the bent perfect Si(111) focusing monochromator [13,14] in the symmetric geometry providing the neutron wavelength of λ=1.55 Å.
The neutron diffraction experiment was mainly focused on the compliance study of the new experimental container. The only one scan of the residual strains near the fracture surface (y = -6mm) was realized in the radioactive CT specimen. The location of measuring points is shown in Fig. 12. The component of the strain tensor perpendicular to the fracture surface was only examined. For comparison, the reference non active CT specimen treated in the same way except the irradiation in reactor was examined as well. The results of diffraction mapping of residual strains are displayed in Fig. 13a,b. Despite of rather deep scan (6mm under the fracture surface) both scans show similar peak of tensile residual strains of the same amplitude of $\boldsymbol{\varepsilon}\sim 3\ 10^{-4}$ located in the vicinity of the final crack tip before rupture. The localization of the strain maximum is slightly different in both examined specimens due to different position of the final crack tip before rupture. Taking into account the corresponding elastic modulus of about 200 GPa, the stress level is roughly estimated as 60 MPa. In the present experiment, a relatively good precision and sensitivity of about $\sim 6\ 10^{-5}$ in strain determination was achieved.
The present experiment with irradiated specimen proved all functions of the newly developed experimental container. The container exhibits a good shielding capacity although full verification of this parameter would be further done with specimens of higher activities approaching the activity limit assumed in construction of the container. In the present case, the average dose rate of 0.4 $mSvh^{-1}$ was measured at the box surface. The mechanical functions of the experimental box in the hot cells were approved as well – easy and safe opening and closing the container, installation of the specimen into the specimen holder by using a mechanical manipulator, remote control of specimen positioning, beam shutters, etc.
The reported experimental facility extends significantly the experimental possibilities on dedicated stress/strain neutron diffractometers in NPI. Application of this technique in evaluation of residual stress level in reactor components in dependence on their operation time and neutron fluence can be very important for assessment of the component integrity and for a support of the operation prolongation.

5. Conclusion

In this contribution, we focused on the physical background and application aspects of the neutron diffraction method of determination of residual stresses in polycrystalline materials. This method has been presented as a very efficient experimental tool, however, higher expenses and the fact that it can be performed at intensive neutron beams (as provided by research reactors or neutron spallation sources) belong to the drawback limiting its wider employment, mainly in technological and engineering applications.

Acknowledgments: This work was supported by the GROWTH program of the Commission of the European Communities under project contract No. G5RD-CT2000-00354, by projects MSM2672244501, AVOZ104805505 and by the research fund of K.U.Leuven within project BIL/05/56. The authors are also grateful to Leif Karlsson (ESAB AB, Goteborg, Sweden) for providing the specimens of WELDOX steels. Authors acknowledge also the attitude of the corrosion group of VGB and very much appreciate the given possibility to use the irradiated specimen for methodological tests of the new experimental facility.

References

[1] M. T. Hutchings, A. D. Krawitz (eds.), Measurement of Residual and Applied Stress Using Neutron Diffraction, NATO ASI Series, Applied Sciences 26 (Kluwer Acad. Publ., 1992).

[2] I.C. Noyan, J.B. Cohen, Residual stress – Measurement by Diffraction and Interpretation, Springer Verlag New York, Berlin, Heidelberg, 1986.

[3] M. Vrána, P. Mikula, P. Lukáš, J. Dubský, V. Wagner, Mat. Sci. Forum 321/324 (2000) 338.

[4] http://www.ujf.cas.cz/

[5] P. Lukáš, M. Vrána, P. Mikula, A. Brožová and M. Ernestová, Proc. of the ICNS 2005, Sydney, Nov. 27 - Dec. 2, 2005, Physica B, in print.

[6] P. Lukáš, P. Šittner, D. Neov, V. Novák, M. Vrána, P. Mikula, Physica B 276/278 (2000) 845.

[7] Y. Tomota, P. Lukáš, S. Harjo, J.H. Park, N. Tsutchida, D. Neov, Acta Materialia, 51 (2003), 819-830.

[8] S. Ueda and M. Gasik, J. Therm. Stress. 23 (2000) 395.

[9] M. Gasik, B. Zhang, Comput. Mech. Sci. 18 (2000) 93.

[10] P. Sarkar, S. Nicholson, J. Am. Ceram. Soc. 78 (1996) 1987.

[11] P. Lukáš, M. Vrána, J. Šaroun, V. Ryukhtin, J. Vleugels, G. Anné, O. Van der Biest and M. Gasik, Mat. Sci. Forum, 492-493 (2005) 201-206.

[12] B. Clausen, T. Lorentzen and T. Leffers, Acta Mater. 46 (1998) 3087-3098.

[13] M. Popovici, W.B. Yelon, J. Neutron Research, 3 (1995) 1.

[14] P. Mikula et al., Physica, B 283 (2000) 289.